Caspian Journal of Mathematical Sciences (CJMS)
University of Mazandaran, Iran
http://cjms.journals.umz.ac.ir
ISSN: 2676-7260
CJMS. **13**(1)(2024), 203-219 (Research paper)

Heat and mass transfer analysis on MHD peristaltic motion of solid particles in a dusty fluid

M. M. Bhatti [1] and A. Zeeshan [2]
[1] Shanghai Institute of Applied Mathematics and Mechanics, Shanghai University, Shanghai 200072, China
[2] Department of Mathematics and Statistics, International Islamic University, Islamabad Pakistan

Abstract. In this study, we investigate the effects of heat and mass transfer on the magnetohydrodynamic (MHD) peristaltic motion of solid particles in a dusty fluid. This analysis encompasses considerations of nonlinear thermal radiation and joule heating. The flow dynamics are modeled for both the fluid and dust phases within the context of a wave frame. We compute solutions for the velocity, temperature, and concentration profiles, analyzing the influence of various physical parameters. Specifically, we examine the impact of particle volume fraction, Hartmann number, Prandtl number, Eckert number, Schmidt number, and Soret number. The mathematical and graphical discussions reveal that both the magnetic field and particle volume fraction exert an opposing influence on the flow. Additionally, it is observed that while the particle volume fraction has a significant effect on the temperature and concentration profiles, these effects are contrasting.

Keywords: Peristalsis, MHD; Heat and Mass Transfer, Solid Particles, Casson Fluid, Thermal Radiation.

2000 Mathematics subject classification: 76W05, 76T20, 80A20; 35Q35.

[1]Corresponding author: mubashirme@yahoo.com
Received: 12 April 2016
Revised: 10 September 2016
Accepted: 29 July 2018

1. Introduction

Heat and mass transfer of solid particles are incredibly common in various engineering and everyday life applications. Water contains a variety of suspended solid particles, air is filled with dust particles, and beverages have particles in the form of bubbles. Furthermore, a wide range of industrial engineering challenges, including the movement of pollutants in water environments, the removal of petroleum residues, and the operation of nuclear nanotechnology reactors, require the use of different carrier fluids to disperse solid particles, droplets, and bubbles. In heterogeneous mixtures with two or more phases, the constituents display a wide range of physical motions and characteristics, each with its own unique velocities. During the flow process of heterogeneous mixtures like particle-fluid suspensions, there is an exchange of mass, energy, angular, and linear momentum. For example, in different heat exchanger scenarios, colder droplets are introduced into condensed vapors. These droplets absorb enthalpy from the vapor, leading to heat transfer. This phenomenon arises from the direct interaction between the vapor and the droplets. Studying the movement of particles in various fluids has posed a considerable obstacle in scientific research for many years.

Living organisms exhibit a fascinating phenomenon where smooth muscles contract and expand symmetrically, resulting in a rhythmic wave-like motion called peristaltic motion. This type of motion plays a vital role in the transportation of different biological fluids within the body. Some examples are ciliary movement, ureteral peristalsis, chyme movement in the small intestines, hydronephrosis, sperm transport, ureteral dilation, gastrointestinal system function, and the movement of artificial calculi. One can make a straightforward assumption about the movement of calculi through a ureteral bolus. Peristaltic motion in the human body happens quite frequently throughout the day, moving a small calculus bolus from the renal pelvis to the bladder within a day. This movement happens within a narrow diameter of about 2.5 mm and at a relatively fast speed of around 3 cm/s, thanks to ureteral peristalsis. Understanding the behavior of calculi in relation to the bladder involves considering the mechanical and physiological challenges posed by their interaction with the ureteral wall structure and surrounding tissues. This contact occurs due to the contraction of smooth muscle tissue, like the ureter, and the force of gravity, which causes solid particles to be propelled through the ureter. The movement of calculi in the ureter is defined by its shape, the process of two-phase flow, and the speed of ureteral peristalsis [1-5].

Peristaltic flow with particle-liquid suspensions has been extensively researched by numerous scientists. In a study conducted by Mekheimer

et al. [6], the peristaltic action of particle-liquid suspensions through a planar channel was investigated. In a study conducted by Nagarani and Sarojamma [7], the researchers examined the movement of small contaminants within a channel using a power law liquid model. In their study, Mekheimer et al. [8] examined the flow of particulate suspensions caused by a sinusoidal peristaltic wave using an eccentric cylinder. Additional analytical and numerical analyses of peristaltic flow and particle-fluid suspensions can be found in references [9-12]. Peristaltic motion with heat and mass transfer is widely utilized in numerous commercial applications. These include heat convection in blood circulation, tissue conduction, food processing, vasodilation, hemodialysis, oxygenation, reverse osmosis, combustion, distillation, and various industrial processes. Several researchers have conducted studies on peristaltic flow with heat and mass transfer. As an illustration, Mekheimer et al. [13] investigated the impact of heat and mass transfer on peristaltic motion in a vertical asymmetric porous channel. In their study, Hayat and Hina [14] examined the impact of heat and mass transfer on MHD peristaltic motion of a non-Newtonian Maxwell fluid with compliant walls. In their study, Hayat et al. [15] investigated the impact of wall properties on the peristaltic flow of a third-grade fluid in a curved channel, specifically focusing on heat and mass transfer. In a study conducted by Ellahi et al. [16], the researchers examined the movement of a viscous fluid in a non-uniform rectangular duct, taking into account heat and mass transfer.

Magnetohydrodynamics (MHD) is also of great importance in various industrial processes and biomedical engineering. The study of Magnetohydrodynamics with heat and mass transfer is important in a wide range of engineering applications, including Hall accelerators, power generators, heating elements, and electric transformers. Understanding the magnetic field's impact on blood flow is incredibly valuable in various medical applications, such as magnetic resonance imaging (MRI), magnetic resonance angiography (MRA), hyperthermia, magnetic drug targeting, and blood pumping. Through precise utilization of pulsating fields and low-intensity magnetic fields, tissue and cell behavior can be effectively altered. The effect of the magnetic field on chyme is reduced by the heat produced by ions in the chyme or the magnetic field. Magnets have been found to have potential benefits in treating various health conditions, including inflammations, bowel diseases, ulceration, and uterine conditions. Peristaltic flow with the combined influences of the Hall current and magnetic field has been extensively studied by numerous researchers. As an example, the study conducted by Hayat et al. [17] examined the combined impact of the Hall and ion slip effects

on the peristaltic motion of a nano-Newtonian Jeffrey fluid model with Joule heating. In their study, Hayat et al. [18] investigated the impact of the Hall current and chemical reactions on the peristaltic flow of a Prandtl fluid with mixed convection. In their study, Eldabe et al. [19] investigated the impact of the Hall current on the peristaltic flow of a Williamson fluid with heat and mass transfer through a porous medium. Additional research on this subject can be found in the cited references [20-22].

This work attempts to investigate the combined impacts of heat and mass transfer on MHD peristaltic flow of solid particles in a dusty fluid, based on the analysis provided above. The governing flow problem is represented in a wave frame, taking into account the assumptions of long wavelengths and a Reynolds number of zero. Analytical solutions are obtained for the ensuing differential equations, and closed-form solutions are provided for both the fluid and dust phases. The structure of this document is as follows: Section 1 serves as an introductory part, Section 2 demonstrates the process of defining the problem, Section 3 explains the approach used to solve the problem, and Section 4 showcases the numerical findings and subsequent discussion.

2. MATHEMATICAL FORMULATION

Consider the peristaltic motion of magnetic solid particles within a dusty Casson fluid, characterized by a velocity denoted as $\tilde{c}$, flowing through a two-dimensional planar channel of uniform thickness. An external magnetic field is applied to this system, while the induced magnetic field is assumed to be negligible due to its relatively small magnitude. A Cartesian coordinate system is employed for the analysis, with the $\tilde{X}$-axis aligned along the centerline of the channel and the $\tilde{Y}$-axis oriented perpendicular to the channel, as depicted in Fig. 1. This configuration allows for a detailed examination of the interactions between the magnetic particles and the fluid flow under the influence of the external magnetic field.

The geometry of the wall surface can be expressed as follows:

$$\tilde{H}\left(\tilde{X},\tilde{t}\right)=\tilde{a}+\tilde{b}\sin\frac{2\pi}{\lambda}\left(\tilde{X}-\tilde{c}\tilde{t}\right). \tag{2.1}$$

In the above equation, $\tilde{t}$is the time,$\tilde{c}$ is the velocity of the wave,$\lambda$is the wave length, $\tilde{a}$is the width of the channel from inlet, and $\tilde{b}$is the amplitude of the wave. The magnetic field is considered of the following form

$$\mathbf{B}=(0,B_0). \tag{2.2}$$

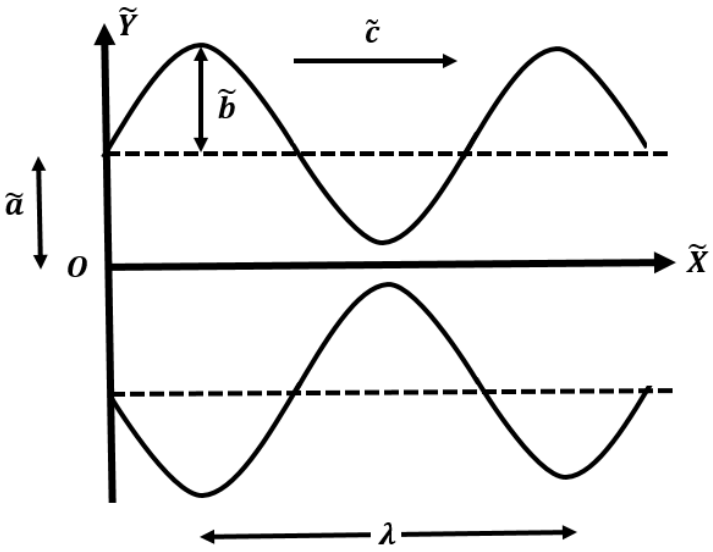

FIGURE 1. Geometric Configuration of Magnetized Casson Fluid Flow with Concurrent Heat and Mass Transfer

With the help of Ohm's Law, we have

$$\mathbf{J} = \sigma \left[\mathbf{E} + \tilde{\mathbf{V}} \times \mathbf{B} \right]. \tag{2.3}$$

In the given equation, σ represents the electrical conductivity, $\mathbf{J}$ denotes the current density, $\mathbf{B}$ represents the magnetic field, and $\mathbf{E}$ represents the electric field. The theory of continuum mechanics states that the equations regulating continuity and linear momentum, along with heat and mass transport for both the fluid phase and the particulate phase, can be represented as follows:

Fluid Phase:

$$\frac{\partial \tilde{U}_f}{\partial \tilde{X}} + \frac{\partial \tilde{V}_f}{\partial \tilde{Y}} = 0, \tag{2.4}$$

$$(1-C)\,\rho_f \left(\frac{\partial \tilde{U}_f}{\partial \tilde{t}} + \tilde{U}_f \frac{\partial \tilde{U}_f}{\partial \tilde{X}} + \tilde{V}_f \frac{\partial \tilde{U}_f}{\partial \tilde{Y}} \right) = -(1-C)\,\frac{\partial \tilde{P}}{\partial \tilde{X}}$$
$$+ (1-C) \left(\frac{\partial}{\partial \tilde{X}} \tau_{\tilde{X}\tilde{X}} + \frac{\partial}{\partial \tilde{Y}} \tau_{\tilde{X}\tilde{Y}} \right) + CS \left(\tilde{U}_p - \tilde{U}_f \right) + \mathbf{J} \times \mathbf{B}, \tag{2.5}$$

$$(1-C)\,\rho_f\left(\frac{\partial \tilde{V}_f}{\partial \tilde{t}}+\tilde{U}_f\frac{\partial \tilde{V}_f}{\partial \tilde{X}}+\tilde{V}_f\frac{\partial \tilde{V}_f}{\partial \tilde{Y}}\right)=-(1-C)\frac{\partial \tilde{P}}{\partial \tilde{Y}}$$
$$+(1-C)\left(\frac{\partial}{\partial \tilde{X}}\tau_{\tilde{Y}\tilde{X}}+\frac{\partial}{\partial \tilde{Y}}\tau_{\tilde{Y}\tilde{Y}}\right)+CS\left(\tilde{V}_p-\tilde{V}_f\right), \tag{2.6}$$

$$(1-C)\,\rho_f c_p\left(\frac{\partial T_f}{\partial \tilde{t}}+\tilde{U}_f\frac{\partial T_f}{\partial \tilde{X}}+\tilde{V}_f\frac{\partial T_f}{\partial \tilde{Y}}\right)=\mathrm{k}\,(1-C)\frac{\partial^2 T_f}{\partial \tilde{Y}^2}$$
$$+\frac{\rho_p c_p C}{\varpi_T}(T_p-T_f)+CS\left(\tilde{U}_f-\tilde{U}_p\right)^2$$
$$+\mu\,(1-C)\,\tau_{\tilde{X}\tilde{Y}}\frac{\partial \tilde{U}_f}{\partial \tilde{Y}}-\frac{\partial q_r}{\partial y}+\frac{\mathbf{J}\cdot\mathbf{J}}{\sigma}, \tag{2.7}$$

$$(1-C)\left(\frac{\partial F_f}{\partial \tilde{t}}+\tilde{U}_f\frac{\partial F_f}{\partial \tilde{X}}+\tilde{V}_f\frac{\partial F_f}{\partial \tilde{Y}}\right)=\mathrm{D_m}\,(1-C)\frac{\partial^2 F_f}{\partial \tilde{Y}^2}$$
$$+\frac{\rho_p C}{\rho_f \varpi_C}(F_p-F_f)+\frac{\mathrm{D_m K}_T}{T_m}(1-C)\frac{\partial^2 T_f}{\partial \tilde{Y}^2}, \tag{2.8}$$

Dusty Phase:

$$\frac{\partial \tilde{U}_p}{\partial \tilde{X}}+\frac{\partial \tilde{V}_p}{\partial \tilde{Y}}=0, \tag{2.9}$$

$$C\rho_p\left(\frac{\partial \tilde{U}_p}{\partial \tilde{t}}+\tilde{U}_p\frac{\partial \tilde{U}_p}{\partial \tilde{X}}+\tilde{V}_p\frac{\partial \tilde{U}_p}{\partial \tilde{Y}}\right)=-C\frac{\partial \tilde{P}}{\partial \tilde{X}}+CS\left(\tilde{U}_f-\tilde{U}_p\right), \tag{2.10}$$

$$C\rho_p\left(\frac{\partial \tilde{V}_p}{\partial \tilde{t}}+\tilde{U}_p\frac{\partial \tilde{V}_p}{\partial \tilde{X}}+\tilde{V}_p\frac{\partial \tilde{V}_p}{\partial \tilde{Y}}\right)=-C\frac{\partial \tilde{P}}{\partial \tilde{Y}}+CS\left(\tilde{V}_f-\tilde{V}_p\right), \tag{2.11}$$

$$\rho_p C c_p\left(\frac{\partial T_p}{\partial \tilde{t}}+\tilde{U}_p\frac{\partial T_p}{\partial \tilde{X}}+\tilde{V}_p\frac{\partial T_p}{\partial \tilde{Y}}\right)=\frac{\rho_p C c_p}{\varpi_T}(T_f-T_p), \tag{2.12}$$

$$C\left(\frac{\partial F_p}{\partial \tilde{t}}+\tilde{U}_p\frac{\partial F_p}{\partial \tilde{X}}+\tilde{V}_p\frac{\partial F_p}{\partial \tilde{Y}}\right)=\frac{C}{\varpi_C}(F_f-F_p). \tag{2.13}$$

In the given equations, $\tilde{U}$ and $\tilde{V}$ represent the velocity components in a fixed frame. ϖ_T represents the time it takes for temperature to relax, ϖ_v represents the time it takes for velocity to relax, and τ represents the stress tensor. The variables $\tilde{X}$ and $\tilde{Y}$ represent Cartesian coordinates in a fixed frame. The symbol ρ represents the density. The term specific heat is denoted by c_p. T represents temperature, F represents concentration, and C represents particle volume fraction. The variable k represents thermal conductivity, while T_m represents the mean temperature.The symbol D_m represents the coefficient of mass diffusivity. K_T represents the thermal diffusion ratio. The subscript f, p indicates the fluid and particle phases.

The mathematical expression for the drag coefficient, as well as the empirical relation for the viscosity of the suspension, are articulated as follows:

$$S = \frac{9\mu_0}{2\overline{a}^2}\widetilde{\lambda}\left(C\right), \widetilde{\lambda}\left(C\right) = \frac{4 + 3\sqrt{8C - 3C^2} + 3C}{\left(2 - 3C\right)^2},$$
$$\mu = \frac{\mu_0}{1 - \chi C}, \quad \chi = 0.07e^{\left[2.49C + \frac{1107}{\overline{T}}e^{-1.69C}\right]}. \tag{2.14}$$

The symbol S represents the drag force, $\overline{T}$ represents the absolute temperature, and $\overline{a}$ represents the radius of the particle. The expression for the radiative heat flux, which is not linear, can be represented as

$$q_r = -\frac{4\overline{\sigma}}{3\overline{k}}\frac{\partial T^4}{\partial \tilde{Y}} = -\frac{16\overline{\sigma}T^3}{3\overline{k}}\frac{\partial T}{\partial \tilde{Y}}. \tag{2.15}$$

The stress tensor for the Casson fluid model is defined as follows:

$$\tau^{1/n} = \tau_0^{1/n} + \mu\dot{\gamma}^{1/n}\ , \tag{2.16}$$

$$\tau_{i,j} = 2e_{i,j}\left(\mu_b + \frac{\wp_y}{\sqrt{2\pi_D}}\right). \tag{2.17}$$

where $\wp_y$ represents the yield stress, π denotes $e_{i,j}$, which is the (i,j) component of the deformation rate, and μ_b stands for the plastic viscosity of the fluid.

Let's establish the transformation variable from the fixed frame to the wave frame as follows:

$$\tilde{x} = \tilde{X} - \tilde{c}\tilde{t},\ \tilde{y} = \tilde{Y},\ \tilde{u}_{f,p} = \tilde{U}_{f,p} - \tilde{c},\ \tilde{v}_{f,p} = \tilde{V}_{f,p},\ \tilde{p} = \tilde{P}. \tag{2.18}$$

Introducing the following non-dimensional quantities

$$\tilde{x} = \frac{x}{\lambda}, \tilde{y} = \frac{y}{\tilde{a}}, \tilde{u}_{f,p} = \frac{u_{f,p}}{\tilde{c}},\ \tilde{v}_{f,p} = \frac{v_{f,p}}{\tilde{c}\delta}, h = \frac{\tilde{H}}{\tilde{a}}, \phi = \frac{\tilde{b}}{\tilde{a}},$$
$$p = \frac{\tilde{a}^2}{\lambda\tilde{c}\mu}\tilde{p},\ \mathrm{Re} = \frac{\rho\tilde{a}\tilde{c}}{\mu},\ \theta_{f,p} = \frac{T_{f,p} - T_0}{T_1 - T_0},\ P_r = \frac{\mu c_p}{\mathrm{k}}, M = \sqrt{\frac{B_0^2\tilde{a}^2\sigma}{\mu}},$$
$$S_c = \frac{\mu}{\rho \mathrm{D_m}},\ S_r = \frac{\rho \mathrm{D_m K}_T}{\mu T_\mathrm{m}}\left(\frac{T_1 - T_0}{F_1 - F_0}\right),\ \Phi_{f,p} = \frac{F_{f,p} - F_0}{F_1 - F_0},$$
$$\mathrm{Ec} = \frac{\tilde{c}^2}{c_p\left(T_1 - T_0\right)}, \delta = \frac{\tilde{a}}{\lambda}, N_r = \frac{16\overline{\sigma}T^3}{3\overline{k}\mathrm{k}}, \zeta = \frac{\wp_y}{\mu_b\sqrt{2\pi_D}}. \tag{2.19}$$

In the given equation, x and y represent the coordinates in the wave frame, u and v represent the velocity components, M represents the

Hartmann number, p represents the pressure, and ϕ represents the amplitude ratio. The Reynolds number, denoted as Re, represents a dimensionless quantity. The variables θ and Φ correspond to the dimensionless temperature and concentration, respectively. The Prandtl number (P_r) represents the ratio of momentum diffusivity to thermal diffusivity. The Eckert number (Ec) quantifies the ratio of kinetic energy to enthalpy. The Schmidt number (S_c) characterizes the ratio of momentum diffusivity to mass diffusivity. The wave number (δ) denotes the spatial frequency of a wave. The radiation parameter (N_r) measures the importance of radiation in heat transfer. The Soret number (S_r) represents the ratio of mass diffusivity to thermal diffusivity.
By substituting Eq. (2.18) and Eq. (2.19) into Eq. (2.1) through Eq. (2.17), and assuming a long wavelength and zero Reynolds number approximation, the resulting equations for the fluid phase can be expressed as follows:

$$\left(1+\frac{1}{\zeta}\right)\frac{\partial^2 u_f}{\partial y^2}-\frac{M^2}{1-C}\left(u_f+1\right)=\frac{1}{1-C}\frac{dp}{dx}, \tag{2.20}$$

$$\left(\frac{1}{\mathrm{P_r}}+\frac{N_r}{(1-C)}\right)\frac{\partial^2\theta_f}{\partial y^2}+\mathrm{Ec}\left(1+\frac{1}{\zeta}\right)\left(\frac{\partial u_f}{\partial y}\right)^2 +\frac{\mathrm{Ec}}{N(1-C)}\left(\frac{dp}{dx}\right)^2+\frac{M^2}{1-C}u_f^2=0, \tag{2.21}$$

$$\frac{1}{S_c}\frac{\partial^2\Phi_f}{\partial y^2}+S_r\frac{\partial^2\theta_f}{\partial y^2}=0, \tag{2.22}$$

For the particulate phase, the equations can be expressed as follows:

$$u_p=u_f-\frac{dp}{dx}\frac{1}{N}, \tag{2.23}$$

$$\theta_f=\theta_p, \tag{2.24}$$

$$\Phi_f=\Phi_p, \tag{2.25}$$

Where $N=\frac{S\tilde{a}^2}{\mu}$.
The corresponding non-dimensional boundary conditions are as follows:

$$\begin{aligned}\frac{\partial u_f}{\partial y}=\ \theta_f=\Phi_f=0 \text{ at } y=0,\\ u_f+1=0,\ \theta_f{=}\Phi_f=1 \text{ at } y=h\left(x,t\right)=1+\phi\sin 2\pi x.\end{aligned} \tag{2.26}$$

3. SOLUTION OF THE PROBLEM

After performing two integrations, the exact solutions for velocity, temperature, and concentration can be expressed in simplified form as follows:

Velocity profile :

$$u_f = -\frac{M^2 + \frac{dp}{dx} - \frac{dp}{dx}\cosh[y\ L_1]\mathrm{sech}[h\ L_1]}{M^2}, \tag{3.1}$$

$$u_p = -\frac{M^2 + \frac{dp}{dx} - \frac{dp}{dx}\cosh[y\ L_1]\mathrm{sech}[h\ L_1]}{M^2} - \frac{dp}{dx}\frac{1}{N}, \tag{3.2}$$

Temperature profile:

$$\begin{aligned}\theta_{f,p} = {} & \frac{1}{8\,(-1+c)\,h{L_1}^2 M^4 n\,(1+N_r(1-C)^{-1}P_r)\,\zeta} \\ & \big[8M^4N(-dp/dxP_r + (C-1)L_1^2(1+Nr(1-C)^{-1}P_r))\zeta \\ & 2L_1^2P_ry(2EchM^4(dp/dx)^2\zeta - 2hM^4N(M^2+dp/dx)\zeta) \\ & +2L_1^2P_r(2hM^4N(M^2+dp/dx)(h-y)\zeta + Ec(dp/dx)^2 \\ & (2hM^4(y-h)\zeta + (C-1)N(1+\zeta))) + Ndp/dxP_r\mathrm{sech}[hL_1] \\ & (8M^4\zeta(1+hL_1\sinh[L_1y]) - (-1+c)EcL_1^2dp/dx(1+\zeta) \\ & \mathrm{sech}[hL_1](2+h(2L_1^2(h-y) - 2L_1^2y) + 2hL_1\sinh[2L_1y]))\big],\end{aligned} \tag{3.3}$$

Concentration profile:

$$\begin{aligned}\Phi_{f,p} = \frac{1}{8h{L_1}^2}\Bigg(& 8{L_1}^2y + L_4S_cS_r\Big(- \big((h-y)(-L_3 + 2hL_1^2(-2L_2+L_3)y)\big) \\ & -8M^4Ndp/dxy\zeta\Big) + L_4S_cS_r\Big(L_3y\cosh[2hL_1] - hL_3\cosh[2L_1y] \\ & +8M^4Ndp/dx\zeta(-h+y+h\cosh[L_1y])\mathrm{sech}[hL_1]\Big)\Bigg).\end{aligned} \tag{3.4}$$

where

$$L_1 = \frac{M\sqrt{\zeta}}{\sqrt{-\left((-1+C)\,(1+\zeta)\right)}},$$

$$L_2 = M^6N\zeta + M^4dp/dx(N - Ecdp/dx)\zeta,$$

$$L_3 = (-1+C)EcL_1^2N(dp/dx)^2(1+\zeta])(\mathrm{sech}[hL_1]^2),$$

$$L_4 = -\frac{P_r}{(-1+C)M^4N(1+N_r(1-C)^{-1}P_r)\zeta}$$

The volume flow rates for the fluid phase and the particulate phase are given by:

$$Q = (1 - C) \int_0^h \tilde{U}_f \mathrm{d}\tilde{Y} + C \int_0^h \tilde{U}_p \mathrm{d}\tilde{Y}. \tag{3.5}$$

The pressure gradient, denoted as dp/dx, is derived upon solving the aforementioned equation. Subsequently, the non-dimensional pressure rise, Δp, is computed numerically using the following expression:

$$\Delta p = \int_0^{2\pi} \frac{dp}{dx} \mathrm{dx}, \tag{3.6}$$

4. RESULTS AND DISCUSSION

In this section, graphical representations of the relevant parameters are presented to elucidate their distinctive characteristics. These parameters include the Hartmann number (M), particle volume fraction (C), Prandtl number (P_r), radiation parameter (N_r), Eckert number (Ec), Schmidt number (Sc), and Soret number (Sr). To this end, Figures 2 through 9 illustrate the pressure rise, temperature profile, and concentration profile. The expression for pressure rise in Eq. (3.6) is determined through numerical computations.

Peristaltic pumping is essential for the movement of different biological fluids in a living organism during peristaltic occurrences. This mechanism is physically demonstrated in the human gastrointestinal tract. The biomedical sector has created various devices utilizing the principle of peristalsis, including roller pumps, the heart-lung machine, and finger pumps. Figures 2 to 5 depict the increase in pressure and the pattern of velocity. Figure 2 clearly demonstrates that an increase in particle volume fraction (C) leads to an enhancement in the pumping rate in the retrograde pumping zone. However, this effect transitions in the peristaltic pumping region and reverses in the co-pumping region. Furthermore, Figure 2 demonstrates that an intensified magnetic field (M) diminishes the increase in pressure in both the co-pumping area and the vicinity of the peristaltic pumping area.

Figure 3 demonstrates that increasing values of the fluid parameter ζ result in a reduction of pressure rise in the retrograde pumping region and an increase in the co-pumping region. Figures 4 and 5 depict the velocity profile. Figure 4 demonstrates that an augmentation in the volume flow rate (Q) results in a corresponding enhancement in the velocity profile. However, the velocity diminishes as the magnetic field (M) increases near the walls. Applying a magnetic field causes a Lorentz force to be produced, which acts against the flow and decreases the speed of the fluid. Figure 5 illustrates that the velocity profile diminishes as the fluid parameter (ζ) increases, but it increases for values of y greater than

0.5. Moreover, an augmentation in the volume percentage of particles (C) substantially amplifies the velocity profile.
Figures 6 through 9 depict the temperature distribution in relation to particle volume fraction, Eckert number, radiation parameter, and Prandtl number. Figure 6 demonstrates that elevated values of particle volume fraction (C) result in an augmentation of the temperature profile. The inclusion of solid particles in a dusty fluid diminishes the thermal efficiency of heat transfer across a channel, leading to elevated temperatures during propulsion. Figure 6 also shows that the temperature falls as the radiation parameter (N_r) increases. Figure 7 demonstrates that the Eckert number (Ec) has a positive effect on the temperature profile. This indicates that kinetic energy is converted into heat through viscous dissipation, resulting in an increase in temperature. The chosen values of the Eckert number for this investigation are suitable, as greater values ($Ec > 2$) indicate compressible flow, which is pertinent to this study.

Similarly, the Prandtl number amplifies the temperature profile, as shown in Figure 7. The Prandtl number, defined as the ratio of thermal diffusivity to momentum diffusivity, indicates that when the Prandtl number is less than 1, thermal diffusivity is greater than momentum diffusivity. This leads to more heat transport in the channel dusty suspension and higher temperatures. Figure 8 demonstrates that increasing values of the Eckert number (Ec) and Schmidt number (S_c) result in a reduction of the concentration profile. The Schmidt number, which represents the ratio of mass diffusivity to momentum diffusivity, plays a crucial role in describing the flow. Figure 9 demonstrates that a substantial impact of the Soret number decreases the concentration profile. Nevertheless, the concentration profile behavior exhibits similarity for the Prandtl number, as depicted in Figure 9.

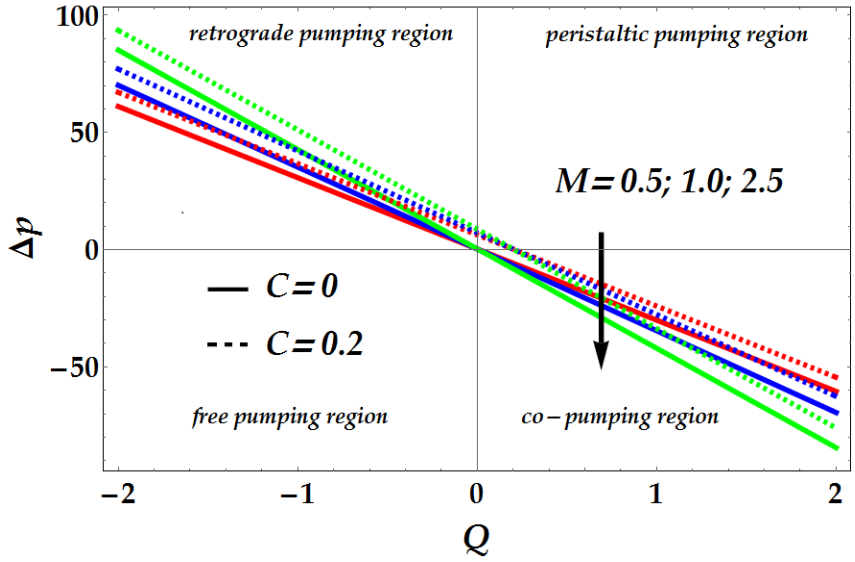

Fig. 2: Correlation between Pressure Increase and Volume Flow Rate for Various Coefficients C and M

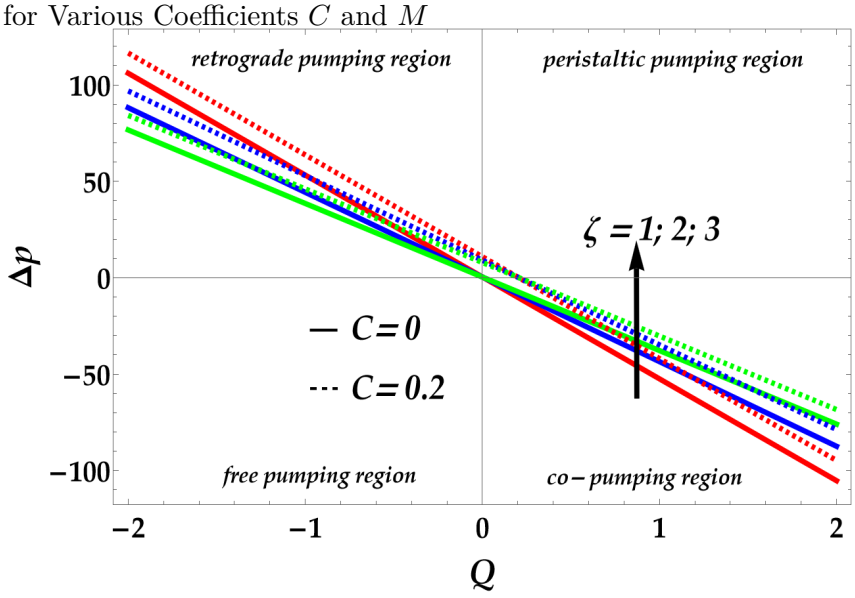

Fig. 3: Relationship between Pressure Increase and Volume Flow Rate for Distinct Values of C and ζ

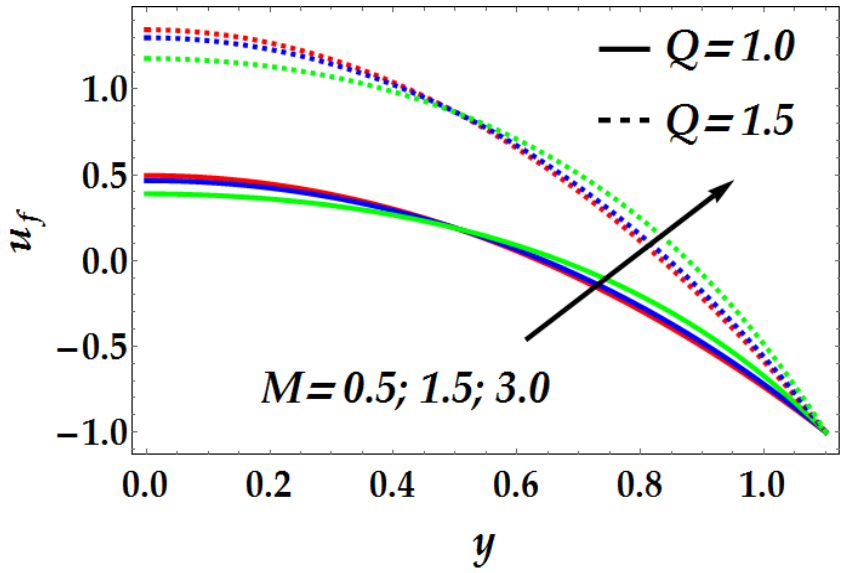

Fig. 4: Velocity Distribution for Different Parameters Q and M

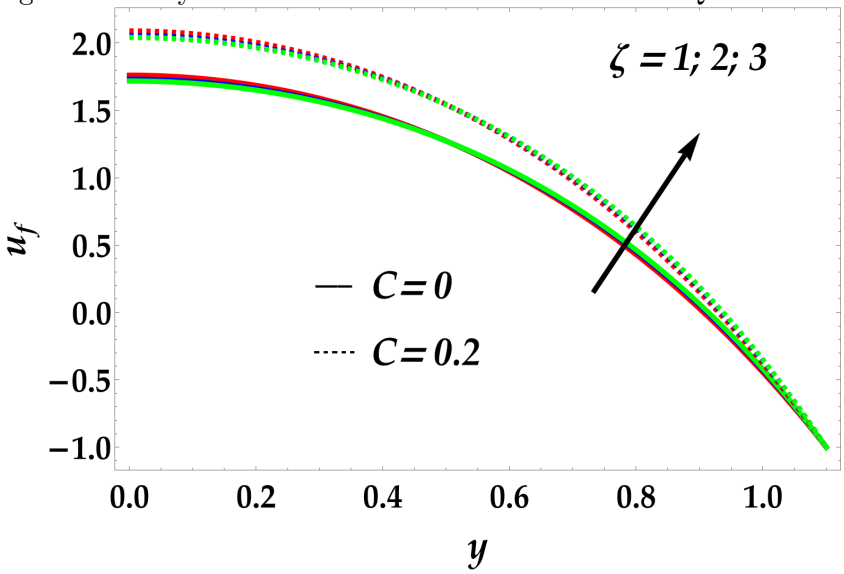

Fig. 5: Velocity Distribution for Various Values of C and ζ

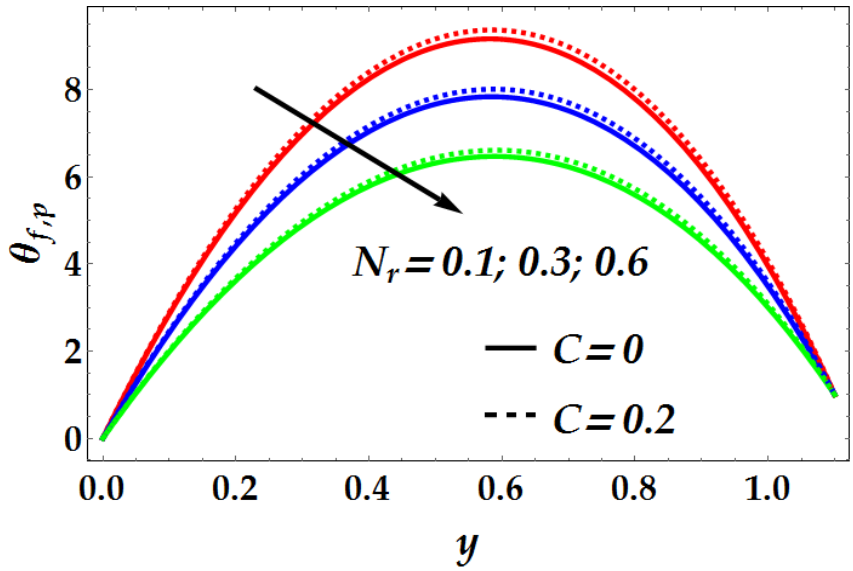

Fig. 6: Temperature Profile for Different Values of C and N_r

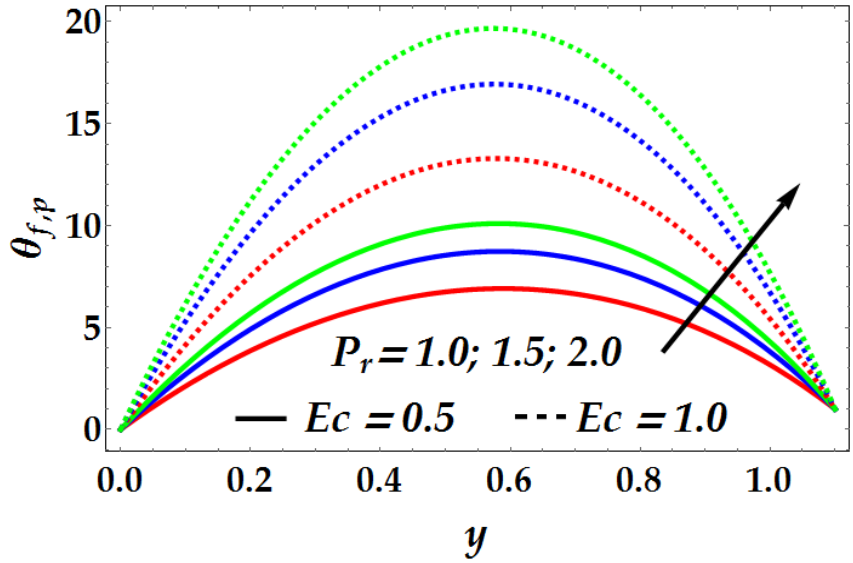

Fig. 7 Temperature distribution for various values of P_r and Ec.

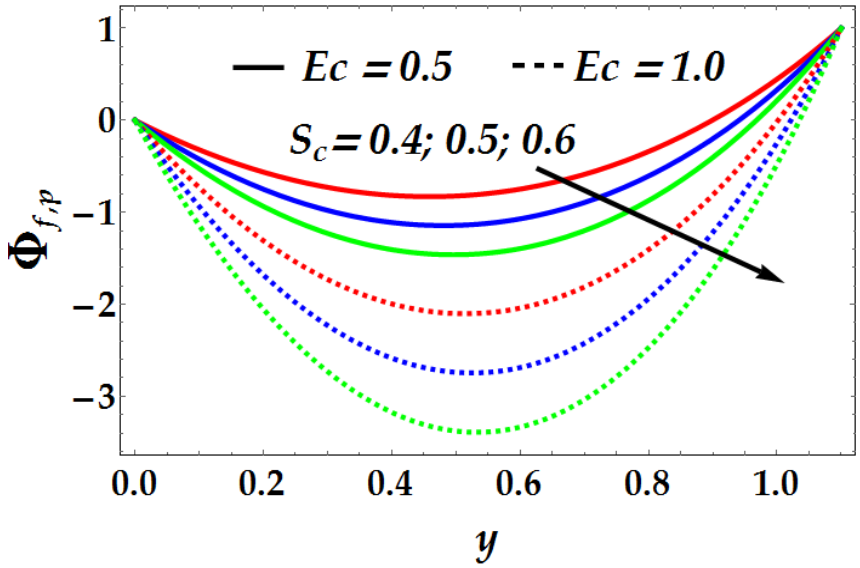

Fig. 8: Concentration Distribution for Various Values of Ec and S_c

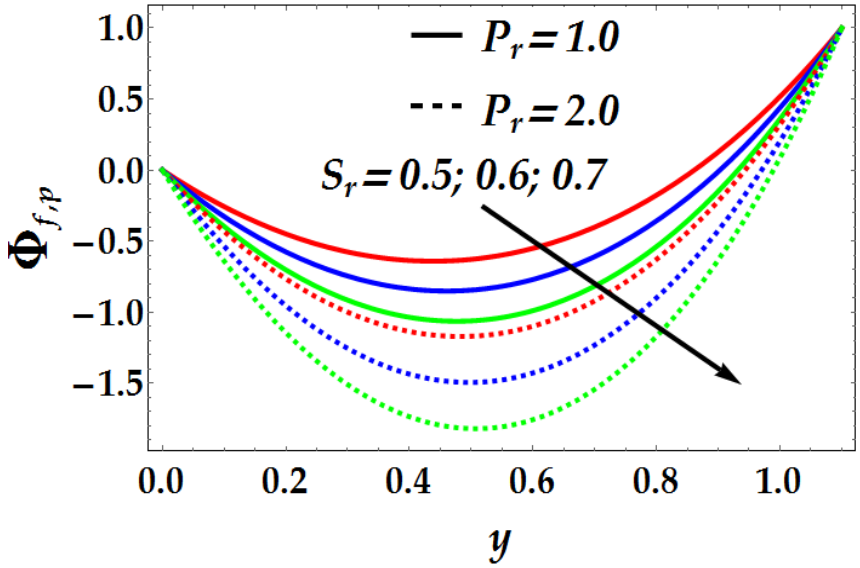

Fig. 9: Concentration Distribution for Different Parameters P_r and S_r

5. CONCLUSIONS

This study investigates the transmission of heat and mass during the movement of solid particles in a dusty fluid, considering the influence of nonlinear thermal radiation and Joule heating in the presence of magnetohydrodynamics (MHD). Velocity, temperature, and concentration

profiles have been determined by analytical solutions, whereas the pressure rise has been calculated using numerical methods. The magnetic field and particle volume fraction have opposite impacts on the velocity profile. To be more specific, a rise in magnetic field strength causes a decrease in velocity, whereas an increase in the fraction of particle volume leads to an increase in velocity. As the radiation parameter increases, the temperature profile decreases because of the greater radiative heat loss. On the other hand, when the amount of particles in the fluid grows, the temperature likewise increases, indicating that particles contribute to the total heating of the fluid. Furthermore, it has been noted that both the Prandtl number and the Eckert number play a role in enhancing the temperature distribution. Therefore, a higher temperature is achieved when there is a greater thermal diffusivity and enhanced viscous dissipation. On the other hand, the Schmidt number and the Soret number cause a reduction in the concentration profile, indicating that higher mass diffusivity and thermal diffusion effects lead to a decrease in solute concentration. Ultimately, the present discoveries can be reduced to those of a Newtonian fluid by allowing the value of ζ to tend towards infinity. This simplification simplifies the complex behavior of the dusty fluid to the more basic dynamics of Newtonian fluids.

References

[1] T.-K. Hung, T.D. Brown, Solid-particle motion in two-dimensional peristaltic flows, J. Fluid Mech. 73 (1976) 77-96.

[2] T.N. Randrianarivelo, G. Pianet, S. Vincent, J.P. Caltagirone, Numerical modelling of solid particle motion using a new penalty method, Int. J. Numer. Methods Fluids 47 (2005) 1245-1251.

[3] J.A.C. Humphrey, Fundamentals of fluid motion in erosion by solid particle impact, Int. J. Heat Fluid Flow 11 (1990) 170-195.

[4] A.V. Catalina, S. Mukherjee, D. Stefanescu, A dynamic model for the interaction between a solid particle and an advancing solid/liquid interface, Metall. Mater. Trans. A 31 (2000) 2559-2568.

[5] J. Li, C. Webb, S.S. Pandiella, G.M. Campbell, Discrete particle motion on sieves—a numerical study using the DEM simulation, Powder Technol. 133 (2003) 190-202.

[6] K.S. Mekheimer, Peristaltic motion of a particle-fluid suspension in a planar channel, Int. J. Theor. Phys. 37 (1998) 2895-2920.

[7] P. Nagarani, G. Sarojamma, Peristaltic transport of small particles — power law fluid suspension in a channel, Australas. Phys. Eng. Sci. Med. 30 (2007) 185-193.

[8] K.H.S. Mekheimer, Y. Abd Elmaboud, A.I. Abdellateef, Particulate suspension flow induced by sinusoidal peristaltic waves through eccentric cylinders: Thread annular, Int. J. Biomath. 06 (2013) 1350026.

[9] M.M. Bhatti, A. Zeeshan, N. Ijaz, Slip effects and endoscopy analysis on blood flow of particle-fluid suspension induced by peristaltic wave, J. Mol. Liq. 218 (2016) 240-245.

[10] M. Ali Abbas, Y.Q. Bai, M.M. Bhatti, M.M. Rashidi, Three dimensional peristaltic flow of hyperbolic tangent fluid in non-uniform channel having flexible walls, Alex. Eng. J. 55 (2016) 653-662.
[11] R. Ellahi, M.M. Bhatti, C. Fetecau, K. Vafai, Peristaltic flow of couple stress fluid in a non-uniform rectangular duct having compliant walls, Commun. Theor. Phys. 65 (2016) 66-72.
[12] R. Ellahi, M.M. Bhatti, A. Riaz, M. Sheikholeslami, Effects of magnetohydrodynamics on peristaltic flow of Jeffrey fluid in a rectangular duct through a porous medium, J. Porous Media 17 (2014) 143-157.
[13] K.S. Mekheimer, S.Z.A. Husseny, Y.A. Elmaboud, Effects of heat transfer and space porosity on peristaltic flow in a vertical asymmetric channel, Numer. Methods Partial Differ. Equ. 26 (2010) 747-770.
[14] T. Hayat, S. Hina, The influence of wall properties on the MHD peristaltic flow of a Maxwell fluid with heat and mass transfer, Nonlinear Anal. Real World Appl. 11 (2010) 3155-3169.
[15] T. Hayat, S. Hina, A.A. Hendi, S. Asghar, Effect of wall properties on the peristaltic flow of a third grade fluid in a curved channel with heat and mass transfer, Int. J. Heat Mass Transf. 54 (2011) 5126-5136.
[16] R. Ellahi, M. Mubashir Bhatti, K. Vafai, Effects of heat and mass transfer on peristaltic flow in a non-uniform rectangular duct, Int. J. Heat Mass Transf. 71 (2014) 706-719.
[17] T. Hayat, M. Shafique, A. Tanveer, A. Alsaedi, Hall and ion slip effects on peristaltic flow of Jeffrey nanofluid with Joule heating, J. Magn. Magn. Mater. 407 (2016) 51-59.
[18] T. Hayat, H. Zahir, A. Tanveer, A. Alsaedi, Influences of Hall current and chemical reaction in mixed convective peristaltic flow of Prandtl fluid, J. Magn. Magn. Mater. 407 (2016) 321-327.
[19] N.T. Eldabe, M.A. Elogail, S.M. Elshaboury, A.A. Hasan, Hall effects on the peristaltic transport of Williamson fluid through a porous medium with heat and mass transfer, Appl. Math. Model. 40 (2016) 315-328.
[20] N.S. Gad, Effect of Hall currents on interaction of pulsatile and peristaltic transport induced flows of a particle-fluid suspension, Appl. Math. Comput. 217 (2011) 4313-4320.
[21] R. Muthuraj, K. Nirmala, S. Srinivas, Influences of chemical reaction and wall properties on MHD Peristaltic transport of a Dusty fluid with Heat and Mass transfer, Alex. Eng. J. 55 (2016) 597-611.
[22] D. Tripathi, O.A. Beg, A study on peristaltic flow of nanofluids: Application in drug delivery systems, Int. J. Heat Mass Transf. 70 (2014) 61-70.